Impedance Spectroscopy of Thin-Film CdTe/CdS Solar Cells Under Varied Illumination

Y. Y. Proskuryakov, K. Durose, and M. K. Al Turkestani
Department of Physics, University of Durham, South Road, Durham, DH1 3LE, UK.

I. Mora-Seró, G. Garcia-Belmonte, F. Fabregat-Santiago, and J. Bisquert
Photovoltaic and Optoelectronic Devices Group, Departament de Física, Universitat Jaume I, 12071 Castell, Spain.

V. Barrioz, D. Lamb, S. J. C. Irvine, and E. W. Jones
Centre for Solar Energy Research (CSER), OpTIC Technium / Glyndŵr University, St. Asaph, LL17 0JD, UK.
(Dated: March 6, 2009)

The electrical properties of CdTe/CdS solar cells grown by metal organic chemical vapor deposition (MOCVD), were investigated by a technique of impedance measurements under varied intensity of AM1.5 illumination. A generalized impedance model was developed and applied to a series of CdTe/CdS cells with variations in structure and doping. The light measurements were compared to the conventional ac measurements in dark under varied dc bias, using the same methodology for equivalent circuit analysis in both cases. Detailed information on the properties of the device structure was obtained, including the properties of the main p-n junction under light, minority carrier lifetime, back-contact, as well as the effect of the blocking ZnO layer incorporated between transparent conductor and CdS layers. In particular, the comparison between samples with different chemical concentration of As has shown that total device impedance and series resistance are strongly increased at lower As densities, resulting in lower collection current and efficiencies. At the same time the minority carrier lifetime was found to be one order of magnitude larger for the lowest value of As density, when compared to the optimized devices.

PACS numbers:

I. INTRODUCTION

It has been recognized recently that impedance spectroscopy methods (used for analysis of electrical properties of a wide range of physical systems), are particularly suitable for in-depth studies of thin-film polycrystalline solar cells [1]. The power of impedance analysis in this case lies in its ability to separate contributions from different layers or regions of a solar cell structure [2]. The method was shown to provide detailed assessment of the device properties, as well as of the possible impact on the overall performance, from each of the device regions individually.

Impedance measurements of thin-film solid state solar cells is an increasingly popular technique, however, the majority of such experiments to date have been carried out almost exclusively under dark conditions [3–6]. On one hand this makes the measurements and interpretation of the spectra easier in some cases. Yet on the other, it also has a strong disadvantage of not providing direct information on a solar cell under its operating condition. In particular, under illumination the distribution of electric fields, as well as the electrical states of defects and impurities (affecting the carrier transport and recombination) are significantly different from those in the dark.

In this work we apply a recently refined technique of impedance spectroscopy carried out under varied intensity of illumination, and compare it with the dark impedance measurements for the case of polycrystalline thin film solar cells. The light technique was successfully applied before to dye-sensitized solar cell systems [7], and more recently to the cells based on microcrystalline and amorphous silicon [2]. Here a series of thin-film devices based on the CdTe/CdS p-n junction and grown by MOCVD [8, 9] is being investigated. The study is focused on the critical aspects of device structure, such as: i) effect from incorporation of a thin barrier layer on device electrical properties and performance; ii) change of properties induced by a variation of the doping level in the p-type CdTe absorber; iii) comparison of impedance characteristics between the samples with and without an extra highly doped CdTe:As layer next to the metal back-contact.

Undoped, low conductivity barrier layers - positioned between transparent conducting oxide (TCO) and window layers - have been recognized over the recent years as an important element of a thin-film cell, contributing to high device efficiencies [10]. The exact effects of such a layer on the internal electrical properties of a solar cell, however, have not yet been fully understood. In this work we carried out the comparison of impedance characteristics from samples with and without a ZnO barrier layer. Also, the comparative approach has been taken for the study of devices p-doped by arsenic at different levels, both in the absorber and contact regions.

II. SAMPLES AND EXPERIMENTAL TECHNIQUE

Four CdTe/CdS samples grown and processed by a MOCVD method have been investigated in this work. Samples I and II have identical and optimized level of doping by As, while differ in structure due to the presence of a ZnO barrier layer in sample I. Sample III has the structure identical to that of sample II, but the level of As doping is considerably smaller, resulting in lower efficiency [8, 9]. Sample IV has the same structure and doping as sample I, but it also contains an extra layer of highly doped CdTe:As at the back contact, which allows for a considerable improvement in efficiency. The details of the employed MOCVD growth procedure can be found in Refs. [8, 9].

The devices consist of commercial indium tin oxide (ITO) glass, 60 nm of ZnO (for samples I and IV), followed by 240 nm of CdS, and further by 4 μm of CdTe doped with As. The MOCVD process was concluded by the growth of a 600 nm thick $CdCl_2$ layer, followed by a 10 minute anneal at 400 ^{o}C under hydrogen [11]. To create a Te-rich layer at the back-surface a conventional bromine-methanol etching step (Br-MeOH, with 0.1% Br) was applied to the CdTe surface for 10 s prior to the evaporation of gold electrodes (samples I-III). In case of sample IV no back-surface etching was applied. However, the concentration of As was raised to 2×10^{19} cm^{-3} for the last stage of the CdTe growth, thus forming a highly doped p-layer of ~ 250 nm.

The solar cell parameters obtained by standard current-voltage measurements under AM1.5 illumination, as well as the parameters of the structure for each device, are summarized in Table I.

The impedance measurements were carried out on Solartron 1260 impedance analyzer, in the frequency range from 0.1 Hz to 300 KHz. Each measurement was done applying a 10 mV ac sinusoidal signal over the constant applied bias. The light source was a 300 W Oriel 81160 solar simulator, with the illumination intensity being varied using neutral density filters. All light measurements have been carried out applying a bias equal to the V_{oc} obtained at each illumination, i.e. under zero current condition. The dark measurements were carried out at a constant dc bias in the range of voltages similar to that for V_{oc}.

III. EXPERIMENTAL RESULTS AND ANALYSIS

A. Impedance spectra and equivalent circuit

Impedance characteristics under light conditions are studied first for the samples with optimized doping level and a basic Au/CdTe back contact structure. Fig. 1 shows examples of impedance spectra of sample I, and Fig. 2 - spectra of sample II, measured at light intensities from 1 sun (100 mW/cm^2) to 10^{-4} sun, at room temperature. The complex spectra are qualitatively similar for both samples, consisting of more than one arc, as seen on the Z''-Z' plots in Fig. 1(a-d) and Fig. 2(a-b).

The right-hand side cut-off of the spectrum on Z' axis corresponds to the total resistance (low frequency impedance) of a device, R_t. Surprisingly, comparison shows that at larger light intensities the R_t values are very close for both of the samples [see Fig. 1(a) and Fig. 2(a)], despite the incorporation of resistive ZnO barrier in sample I. At low light intensities ($< 10^{-3}$ sun), the situation changes and R_t becomes significantly larger, as one could expect, for sample I [by a factor of ~ 1.5, Fig. 2(b)].

To assess the exact contributions of the circuit elements into spectra at different light intensities, a number of equivalent circuits has been studied according to the procedure outlined in Ref. [1]. The simplest consists of two parallel assemblies of R-C elements, and is shown in Fig. 3(a). It produces two adjacent semiarcs on Z''-Z' plot – see dashed lines in Fig. 1(a) and Fig 2(a). This circuit represents the most simple model of a CdTe/CdS p-n junction (R_1-C_1) in series with a Schottky junction formed at the back-contact (R_2-C_2) [6]. From our analysis it has been found, however, that a circuit of two section only is incapable of self-consistently describing the entire data sets. Also, a spatial inhomogeneity, probably originating from grain boundaries in the absorber layer, made it necessary to introduce a CPE (constant phase elements) in parallel with the capacitance of the p-n junction [13] (CPEs are used to represent a distribution of circuit element values in an equivalent circuit). The final circuit consisting of three sections is shown in Fig. 3(b).

Ref. [1] explains how, for the case of CdTe/CdS solar cells, certain plots of admittance data are more sensitive to variations in the equivalent circuit parameters than others. The coordinates best used for fitting models to experimental data in this case are known to be: i) the Z''-Z' plot, ii) the frequency dependence of capacitance C (i.e. E', the real part of the dielectric permittivity), and iii) the frequency dependence of the imaginary part of the electric modulus M'' [1].

In Fig. 1(e-h) and Fig. 2(c-d) the same data that has been shown on $Z'' - Z'$ plots [Fig. 1(a-d) and Fig. 2(a-b)], are plotted as the frequency dependances of $E'C_S = C$ (left axis) and M''/C_S (right axis), where C_S is the capacitance of the sample holder. Solid lines in Figs. 1 and 2 are fits to the equivalent circuit shown in Fig. 3(b). Good agreement is obtained for entire data sets in the range of light intensities from 1 sun to 10^{-4} sun.

TABLE I: Device parameters for the four studied solar cells. N_{As} is the chemical concentration of As in the CdTe layer, η - cell efficiency, V_{oc} - open circuit voltage, J_{sc} - short circuit current.

Samples	N_{As} (cm^{-3})	ZnO	Back-contact	η (%)	V_{oc} (V)	J_{sc} ($\frac{mA}{cm^{-2}}$)	FF (%)
I	2×10^{18}	Yes	Au/CdTe	8	0.6	20.5	61
II	2×10^{18}	No	Au/CdTe	6.5	0.58	18.3	57
III	1×10^{17}	No	Au/CdTe	1.5	0.5	4.4	65
IV	2×10^{18}	Yes	Au/As^{+}doped/CdTe	10.5	0.72	21.3	70

B. Analysis of extracted parameters

The extracted values of the equivalent circuit parameters are plotted in Fig. 4 as functions of the open circuit voltage V_{oc} (measured at each given light intensity I, $V_{oc} \propto \ln(I/I_0)$, where I_0 is a constant). It is seen that the elements corresponding to the second and third sections of the circuit, Fig. 4(c-h), are quite close for both samples I and II. This clear correlation supports the validity of the fitting procedure. The distinct difference between the parameters for the first section of the two samples [see Fig. 4(a-b)] is explained in Section III B1 below.

Fig. 4(i) shows plots of the characteristic times for the first and third sections $\tau_0 = R_0C_0$ and $\tau_2 = R_2C_2$. Both τ_0 and τ_2 behave similarly in samples I and II. However, the two time constants differ from one another by a factor of 5. This difference can be expected since the two represent the charging/discharging events in deferent areas of a device.

1. *First section of equivalent circuit, R_0-C_0*

The difference in the behavior of the parameters $C_0(V_{oc})$ and $R_0(V_{oc})$ for samples I and II [see Fig. 4(a-b)], is clearly related to the influence of the incorporation of the ZnO layer, as the devices are otherwise similar. This suggestion is verified by the observed behavior of the resistance R_0: its values are significantly lower for sample II than for sample I over the large part of the V_{oc} range, Fig. 4(b). It has been shown in Fig. 2(b) that near dark the total device resistance (R_t) is larger for sample I containing ZnO, which also correlates with the results of Fig. 4(b). Interestingly, the values of R_0 at intensities ~ 1 sun are very close for the two devices, indicating that the blocking effect of ZnO layer is negligible under these conditions. The later corresponds to the general observation of increased efficiency in devices containing a barrier layer. The origin of the apparent drop of ZnO resistivity under 1 sun is not clear at this stage, but it can be suggested that it is caused by the injection of photogenerated electrons into ZnO from the main junction.

The magnitude of capacitance C_0 for sample I does not change significantly in the studied V_{oc} range. It corresponds to a characteristic length $d \sim 400$ nm, obtained using flat plate capacitance relation, and taking standard values for dielectric permittivity of ZnO and CdS as ~ 10. This value is comparable to the sum of thicknesses of ZnO (60 nm) and CdS layers (240 nm), implying that it can be associated with the geometrical capacitance. On the other hand, variation of C_0 with V_{oc} in sample II shows that in this case the associated device region is electrically active. The origin of this variation can be interface states (between TCO and CdS) which are discharged under illumination, and thus resulting in the decrease of C_0 towards the geometrical value. It is possible to suggest in this scenario, that ZnO layer plays a passivating role - suppressing the effects of interface states.

2. *Second section of equivalent circuit, R_1-C_1*

In Fig. 4(j) the characteristic time for the second section, $\tau_1(V_{oc}) = R_1C_1$, is plotted. It is seen that τ_1 is almost constant at $V_{oc} > 0.4$ V and of approximately the same value for both samples. For linear recombination, diffusion capacitance and recombination resistance have opposite (linear and reciprocal) dependence on carrier density, due to the accumulation of carriers in the absorber layer. Thus their product, which is equivalent to minority carrier lifetime, is expected to be rather independent of the degree of illumination and V_{oc} [15]. From plots in Fig. 4(j) it is seen that such a description is well applicable, hence we can attribute C_1 to diffusion capacitance [14], and R_1 to the recombination resistance of the absorber layer under illumination. The magnitude of the minority carrier lifetime ($\tau_1 \sim 1$ μs) agrees with the value expected for a highly doped CdTe solar cell [16].

3. *Third section of equivalent circuit, R_2-C_2*

The third section of equivalent circuit can be attributed to the back contact. This is supported by the fact that the structure of this region of the device is expected to be the same for samples I and II, while results in Fig. 4(g-h) show that the respective parameters are indeed very similar in the two samples. Fig. 4(g) shows that the value of C_2 at low light or dark is ~ 0.8 nF, that corresponds to a depletion length of 365 nm, and is comparable to the previously reported value (~ 0.5 μm) for a Au/CdTe back-contact [1]. Under 1 sun the depletion length decreases to ~ 30 nm, while R_2 decreases by two orders of magnitude, Fig. 4(h).

At the region adjacent to the back-contact it is the number of majority carriers only that is increased under illumination, as all electrons are expelled towards the front contact by the charge separation. It is essential to point out, that in the present situation the back contact region is under zero dc bias, as zero current condition is maintained. At the same time the Schottky diode at the back surface does not generate any photovoltage by itself, as all the light is absorbed at the front. Therefore the only possibility in which light absorbed in the main junction can exert the influence on the back-contact parameters is via an increase of the majority carrier density in that region by diffusion [18].

C. Comparison with dark measurements

There is a common notion regarding impedance properties of solid state solar cells, that measurements in light and dark are in many respects equivalent, as in being able to provide the dc bias characteristics of the same magnitude in both cases. This largely stems from classical studies on properties of silicon solar cells. In particular, the dc bias characteristics extracted from impedance measurements, either in light or dark, are usually expected to provide similar values of minority carrier lifetime. [19]

On the other hand, in the area of polycrystalline thin-film devices based on CdTe or $CuInGaSe_2$ materials, the main focus to date has been on impedance studies in the dark only, while no investigations under varied-illumination have been carried out. In order to make the comparison with the data obtained under illumination described in previous sections, impedance measurements under varied dc bias in the dark are now considered.

The obtained dark impedance spectra for samples I and II (not shown) have been found to be qualitatively similar to those in the light, Fig. 1 and Fig. 2. The equivalent circuit of Fig. 3(b) has been also found to describe the dark data very well. In Fig. 4 the parameters extracted for sample I are plotted as functions of the applied dc bias (grey triangles). It is seen, that the dark parameters overall show similar characteristics (compare with light values for sample I, shown by black squares), however, significant deviations occur in resistance R_0 (at $V_{dc} \gtrsim 0.5$ V), and in C_1 and CPE_1 values. The dark values of C_2 and R_2 appear to coincide with the light values in the entire voltage range. At the same time the obtained values of dark minority carrier-lifetime, Fig 4(j), are approximately an order of magnitude larger than the light values. It is logical to suggest that this difference originates from the change in the population of the charged defect states caused by illumination. This can also be the reason for the difference between light and dark values of parameters C_1 and CPE_1.

In terms of analysis, the main difference between the set-ups for light and dark measurements is that in the latter case a potential divider relation should be applied, due to the non-zero current condition. (I.e. in this case a series assembly of resistances R_0, R_1 and R_2 forms a load for the applied dc bias. The total dc voltage applied is then divided into three potential drops across the respective regions of the device.) At the same time, in light the main junction (section 2 of the equivalent circuit) can be considered as a voltage source V_{oc}, while resistors R_0 and R_2 have zero voltage drops across them, as there is no current.

Using potential divider for the dark measurements, based on the obtained values of resistances R_i (i = 0, 1, 2), it was found that voltage across R_0 provides a significant contribution into V_{dc} at $V_{dc} \gtrsim 0.5$ V. This can explain the observed difference in R_0 mentioned above. There is no substantial difference between compared values of C_0, as this parameter shows only small variation with voltage either in light or dark. The voltage across R_1 (V_1) provides a significant contribution into V_{dc}, while overall the dark characteristic $\tau_1(V_1)$ is similar to that shown in Fig. 4(j).

The voltage drop across R_2 has only a weak variation with V_{dc} and remains smaller than 0.12 V. Thus, for section R_2-C_2 the situation in dark resembles that of the open circuit condition in the light measurements (no bias across R_2), which explains the similarity in both cases, Fig. 4(g) and Fig. 4(h).

D. Impedance data for sample III (reduced absorber doping)

The examples of impedance spectra for sample III are shown in Fig. 5. The Z''-Z' spectra differ in shape from those of samples I and II, while the total resistance R_t is overall much larger than that in the previous cases. However, because sample III has exactly the same structure and growth parameters as sample II (apart from N_{As}), the equivalent circuit shown in Fig. 3(b) is a valid candidate in this case also. Solid lines in Fig. 5 represent the best fit obtained using this model, and the obtained fitting parameters are shown by crosses in Fig. 4. It can be concluded, both from the quality of the fit as well as from the good correlation of the extracted parameters with those of samples I and II, that this model is indeed valid.

The values of parameters R_2 and C_2, corresponding to the back-contact are very close to the values obtained in all of the cases considered so far [Fig. 4(g-h)]. This supports the interpretation of the third section in the studied equivalent circuit, given that the structure of the back-contact is identical to samples I and II. The overall behavior of R_0 and C_0 follows that of sample I with the ZnO layer, despite the fact that sample III does not contain ZnO. This can indicate that increased As doping can have a passivating effect on charged states similar to that of a ZnO layer. R_1 in sample III is very close to that in other samples, while C_1 is considerably larger, Fig. 4(c-d). This results in the minority carrier lifetime ($\tau_1 = R_1 C_1$) being approximately an order of magnitude

larger than in samples I and II, Fig. 4(j).

E. Impedance data and equivalent circuit for sample IV (barrier layer plus doped contact)

The examples of impedance spectra obtained on sample IV are shown in Fig. 6. The spectrum at 1 sun has complex shape and is similar to that of sample I, Fig. 6(a). At lower light intensities, however, it very quickly becomes dominated by a single arc shape, until almost a perfect semicircle is obtained at near dark, Fig. 6(b).

The analysis has shown that to describe these spectra satisfactorily, the equivalent circuit of only two R-C sections is needed; while section R_2-C_2 in the equivalent circuit [Fig. 3(b)] can be substituted by the fixed value resistor $R_2 \sim 20$ Ohm, due to the improvement of the back-contact. It was also found that capacitance C_1 was not necessary in this case, so that the circuit is reduced to the simplified form shown in Fig. 7(a). The effective junction capacitance C_1^* is then calculated from the obtained CPE_1 values according to the procedure that is described in the Appendix.

Fig. 7(b) shows the comparison of impedance spectra at 1 sun between sample I and sample IV. It is seen that the overall impedance of sample IV is strongly decreased by the optimization of the back-contact. Fits of good quality to the spectra were obtained using the model in Fig. 7(a), and are shown by solid lines in Fig. 6. The extracted parameters are shown in Fig. 8 by solid symbols.

Until this point the potential spatial inhomogeneity of the sample region, represented by the first section C_0-R_0, has been neglected. However, we have also carried out a fitting procedure substituting capacitance C_0 by a constant phase element CPE_0. In this case the effective capacitance C_0^* was obtained in the same manner as effective capacitance C_1^* (see Appendix). The quality of the fit is similar to the previous case, and the obtained fitting parameters are shown in Fig. 8 by open symbols. It is seen that both approaches give very similar results. Moreover, the obtained values of the parameter $CPE_0 - P$ vary between 0.95 and 1 ($CPE - P = 1$ corresponds to an ideal capacitor, $CPE - T = C$), which proves that spatial inhomogeneity is very small in this case and can be neglected.

It is seen in Fig. 8(a), that capacitance C_0 for sample IV shows practically no variation, just as C_0 in sample I, Fig. 4(a). This could be expected, as both samples contain ZnO layer. The parameter $CPE_1 - T$, as well as the associated capacitance C_1^*, shows weak variation under lower light intensities. At larger intensities, $V_{oc} \gtrsim 0.65$ V, a transition to exponential dependance takes place. It can be suggested that this occurs when the diffusion capacitance starts dominating over the depletion capacitance, similar to the case of Si solar cells [19].

The possible reason why the depletion capacitance is not clearly defined at low V_{oc} values for other samples [Fig. 4(c)], can be found in the parallel association of CPE_J and C_1, chosen to represent the total capacitance of the junction. In this case one can assume that C_1 expresses the contribution from the diffusion capacitance, whilst the CPE_J most likely expresses the depletion contribution. Although it is not straightforward why such separation of the contributions occurred for samples I–III, it is not unnatural. It agrees with the fact that depletion and diffusion parts always contribute into total junction capacitance via parallel association. Also, the diffusion capacitance might be less affected by the spatial inhomogeneity than the depletion part. Hence the former is characterized by C rather than a CPE in the equivalent circuit.

In Fig. 8(h) the characteristic time $\tau_1^* = R_1 C_1^*$ is plotted. After an initial decrease it saturates at $V_{oc} > 0.65$ V to the value of $\sim$ 3 μs, with a slight upturn at $V_{oc} > 0.72$ V.

Because the diffusion capacitance dominates at $V_{oc} \gtrsim 0.65$ V, we conclude that the averaged value of τ_1^* in the same region corresponds to the minority carrier lifetime. It should be mentioned also, that the characteristic time only has the physical meaning of lifetime when the capacitance employed in its calculation is the diffusion capacitance. The obtained value of averaged τ_1^* ($V_{oc} \gtrsim 0.65$ V) is comparable to the value of minority carrier lifetime observed in samples I and II: $\tau_1 \sim 1.5$ μs.

IV. DISCUSSION

A. Total and series resistance

From the comparison of τ_1 in samples I–III, Fig. 4(j), it can be concluded that the magnitude of minority carrier lifetime is reduced by the increase of the chemical concentration of As. At the same time this implies that it is not τ_1 that is limiting the device performance as efficiency of sample III is lowest.

On the other hand I-V measurements show that current collection (J_{sc}) is strongly reduced at lower N_{As} (sample III), pointing out that carrier mobility and device series resistance can be the major factors limiting device efficiency.

The data for resistance values from different sections of a device, Fig. 4 and Fig. 8, allow calculation of the contribution to the series resistance of the cell from the contact regions as: $R_s = R_0 + R_2$, and the total resistance as $R_t = R_s + R_1$. In Fig. 9 R_t and R_s are plotted for samples I–IV. For samples I and II the values of both of the parameters R_t and R_s are very close at light intensities from $\sim$ 0.1 to 1 sun. This suggests an important conclusion, that under sufficient illumination ZnO layer does not make a detrimental contribution to the series resistance or carrier mobility. In the same intensity range, for sample III, R_t and R_s are, respectively, factors of three and two larger than in samples I–II; while for sample IV - these parameters are lower by the same factors.

Because the influence of ZnO layer on both R_t and R_s can be considered as negligible, the observed differences between samples can be attributed to the effect of As doping alone.

Sample III has the lowest chemical concentration $N_{As} = 1 \times 10^{17}$ cm^{-3}, while three other samples have the concentration of 2×10^{18} cm^{-3}. At the same time the net concentration of electrically active acceptors (determined by C-V) is comparable in all of the cases, $p \sim 1 \times 10^{14}$ cm^{-3}) [9]. Thus, from comparison in Fig. 10, it can be concluded that enhanced As concentration reduces series resistance, but not by a doping action as such. More likely, this occurs via reduction of the resistance of interfaces such as grain-boundaries, where accumulation of excessive As is possible. On the other hand, further improvement in R_t and R_s takes place after reduction of the back-contact resistance via additional doping, as is seen from comparison with sample IV.

B. Recombination and carrier trapping in CdTe absorber layers

As it was discussed in the previous section, one of the roles of the element CPE_J (or CPE_1 in case of sample IV) is to account for the depletion capacitance. Another role of this element is to represent the spatial (statistical) distribution of the junction capacitance in general. This distribution can originate from grain boundaries and structural imperfections, as well as it can be caused by charged impurities within the absorber layer.

In the previous study a set of several well resolved deep states has been detected in a commercial CdTe/CdS solar cell [17]. These states were self-consistently incorporated into total equivalent circuit of the device in dark [1]. The number of such deep states, however, can be arbitrary and depends on the sample growth and processing conditions. It was shown in Ref. [20], that if the number of states is large, i.e. they form a broad distribution of the trapping states, the multitude of their individual contributions into a device equivalent circuit can reduce to a single CPE. This is a result of the multiple trapping (MT) model, which was found to describe the effects of such broad trap distributions on the carrier transport in amorphous materials and also die sensitized solar cells [20, 21].

The relevance of the MT description to the studied here devices can be seen from the previous study of the densities of states for samples I and II [12]. There, a very broad distribution of deep states was obtained for both of the samples, with the range of trap energies varying from 0.4 to $\sim$ 1 eV. It is thus conceivable, that the MT mechanism can be relevant to the studied samples, and that the contribution of the deep states into equivalent circuit can also occur via the constant phase element. In this case the transport of electrons in the conduction band is effectively slowed down by the trapping-detrapping events. The effective minority carrier lifetime τ_1^* (obtained using a CPE) is then expected to be larger than the lifetime of electrons in the conduction band (represented by τ_1 in our case), as indeed can be seen comparing the data in Fig. 4(j) and Fig. 8(h): $\tau_1 \sim 1.5$ μs and $\tau_1^* \sim 3$ μs.

V. CONCLUSION

A series of CdTe/CdS solar cell devices with varied chemical concentration of As as well as structural variations have been studied by impedance spectroscopy under illumination from 1 sun to 10^{-4} sun. A generalized equivalent circuit model which describes the structure and operation of the devices has been established. In particular it has been found that three samples in the series are described by exactly the same circuit model despite the variation of the structure and doping. The forth device, with an improved back-contact, has been described by a simplified variant of the same circuit, also showing a good correlation in the parameters obtained with those in the other devices.

The study of the effect of varied arsenic concentration has shown that carrier mobility and series resistance are the major factors affected by such doping of the CdTe, as well as the main factors affecting efficiency. Importantly, the effect on R_s from increased As level is caused not by the doping action as such, but rather is due to the accumulation of As at the interfaces and grain boundaries. On the other hand, the minority carrier lifetime is increased in devices with lower As level, presumably due to lower disorder, however, the device efficiency is still strongly reduced due to the accompanying increase of R_s. The ZnO incorporation has been found to produce no effect on the device impedance and series resistance under 1 sun illumination, while producing significant contribution into R_t and R_s at lower intensities. High CdTe:As doping at the 'back-contact' has been found to reduce dramatically the total impedance and series resistance.

Impedance measurements in the dark were carried out under varied dc bias and compared with the light measurements. It was shown that data obtained at non-zero current conditions are much more complex for analysis as compared to that from the zero-current light measurements. The values of minority carrier lifetime obtained in light and dark were found to differ by one order of magnitude. The suggested origin of this difference is the alteration of a particular charge state of impurities and grain boundaries, induced by illumination. It was thus established that for polycrystalline thin-film solar cells the impedance measurements in the light (in the open circuit condition) is the preferred experimental method for equivalent circuit characterization.

VI. APPENDIX: EFFECTIVE CAPACITANCE OF A $R-CPE$ SECTION

The characteristic time of a process represented by an arc or semicircle in impedance is determined by the inverse of frequency at which the maximum in $-Z''(Z')$ is attained. In this sense, for the circuit consisting of a single R-C parallel assembly, the impedance can be described as:

$$Z'_{R-C} = \frac{aR}{a^2+b^2}, \text{ and } -Z''_{R-C} = \frac{bR}{a^2+b^2} \qquad (1)$$

Where $a = 1$, and $b = \omega CR$. Then the maximum of the imaginary part can be found at $\omega_{\max}$:

$$\left(\frac{\partial - Z''}{\partial \omega}\right) = 0, \;\Rightarrow\; \omega_{\max} = \frac{1}{RC}, \qquad (2)$$

and here $\tau = RC$ is the characteristic time.

In case of a single R-CPE parallel assembly, a depressed semicircle represents its spectrum on Z''-Z' plot [13], while the total impedance of such circuit is given by:

$$Z_{R-CPE} = \left(\frac{1}{R} + (j\omega)^n Q\right)^{-1}, \qquad (3)$$

where $Q = CPE - T$, $n = CPE - P$, and $j = \sqrt{-1}$. Now applying Eq. 2 to Eq. 3 we find,

$$\omega_{\max} = \tau^{-1} = (QR)^{1/n}. \qquad (4)$$

Comparing Eq. 2 and Eq. 4, one can see that effective capacitance C^* for a R-CPE circuit can be defined as:

$$C^* = \frac{(QR)^{1/n}}{R}. \qquad (5)$$

Eq. 5 describes the approach used for determination of equivalent capacitances C_0^* and C_1^* in sample IV, as mentioned in Section III E.

Fig. 1

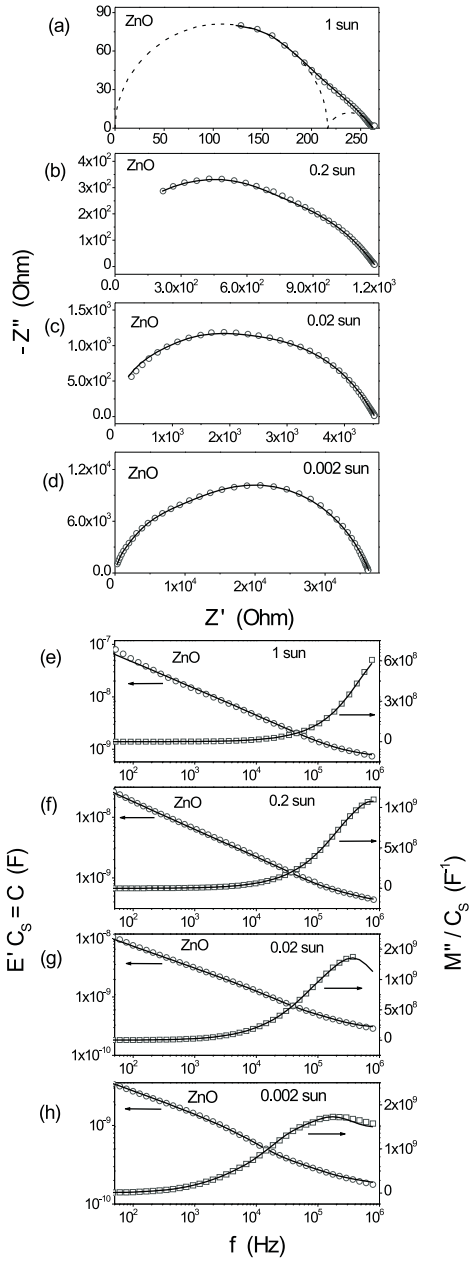

FIG. 1: (a-d) Impedance spectra on a Z''-Z' plot for sample I under varied light intensity in the range from 1 sun to 0.002 sun. (e-h) The same impedance data represented as real part of dielectric permittivity E' and imaginary part of electric modulus M'' versus frequency. In all plots: solid lines - fit to the model in Fig. 3(b). Dashed lines in (a) depict spectrum from the two-section circuit of Fig. 3(a).

Fig. 2

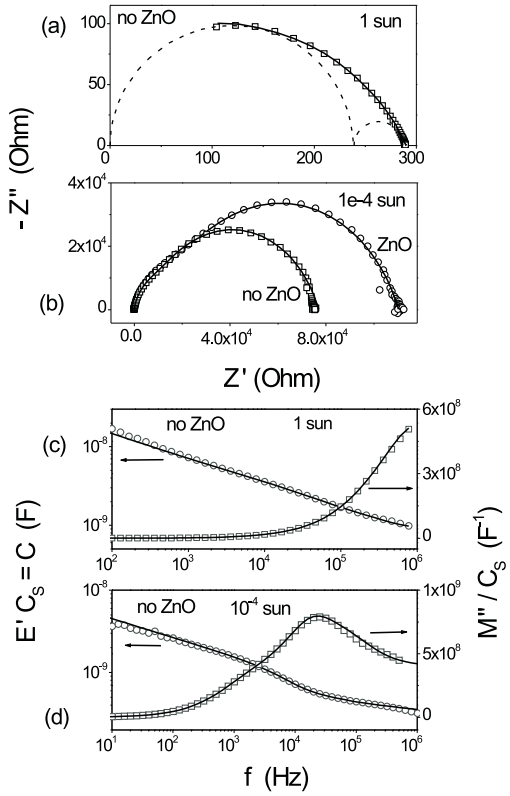

FIG. 2: (a) Impedance spectra on a Z''-Z' plot for sample II under light intensity of 1 sun. (b) Z''-Z' data in near-dark condition for sample I and II (light intensity of 10^{-4} sun). The spectra coincide in the high frequency part (at low Z'). (e-h) The same impedance data for sample II as in (a-d), represented as $E'(f)$ and $M''(f)$. In all plots: solid lines - fit to the model in Fig. 3(b). Dashed lines in (a) depict spectrum from two-section circuit of Fig. 3(a).

Fig. 3

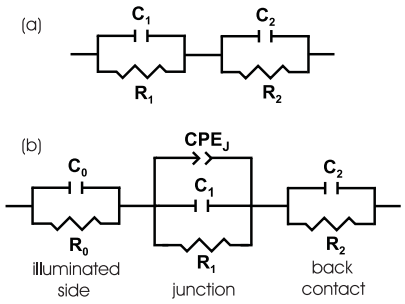

FIG. 3: (a) Basic equivalent circuit of a p-n type solar cell with a Schottky barrier at the back contact. (b) Refined equivalent circuit which was found to describe impedance data of the studied CdTe/CdS samples under various illumination conditions.

Fig. 4

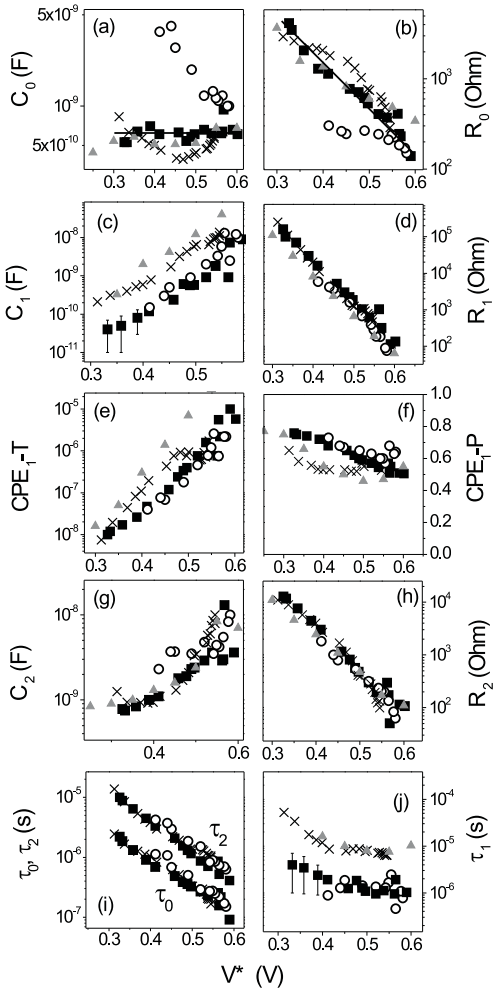

FIG. 4: (a-h) Equivalent circuit parameters obtained using model in Fig. 3(b), plotted as functions of the open circuit voltage ($V^* = V_{oc}$ for light data, $V^* = V_{dc}$ for dark data). (i) Characteristic times τ_0 and τ_2 for the first and third sections of the equivalent circuit. (j) Minority carrier lifetime obtained as $\tau_1 = R_1 C_1$, using data in (c) and (d). Solid squares - values obtained for sample I (with ZnO), open circles - for sample II (no ZnO), crosses - sample III (all three plotted against V_{oc}); grey symbols - dark values for sample I (plotted against V_{dc}). The lines are a guide for the eye. Note that V_{oc} approximately follows the $\log(I)$ dependence, where I is the light intensity.

Fig. 5

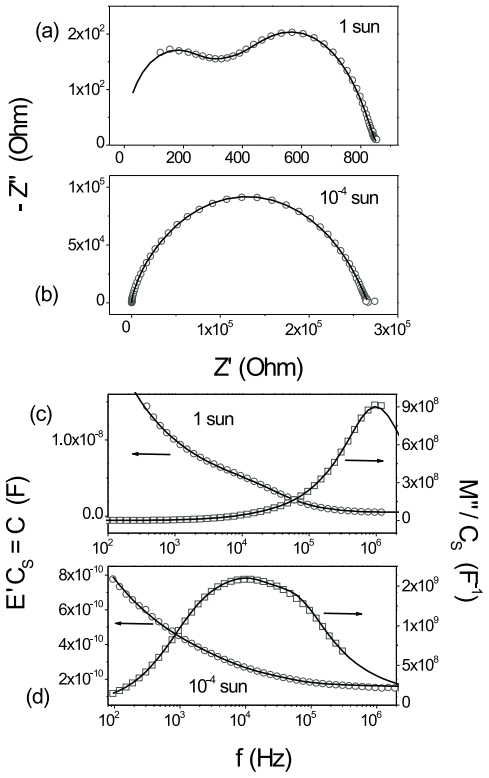

FIG. 5: Examples of impedance spectra on a Z''-Z' plot for sample III under illumination; at 1 sun - in (a), and at 10^{-4} sun - in (b). (c-d) Real part of dielectric permittivity E' and imaginary part of electric modulus M'' versus frequency at the same light intensities. Solid lines are fit to the model in Fig. 3(b).

Fig. 6

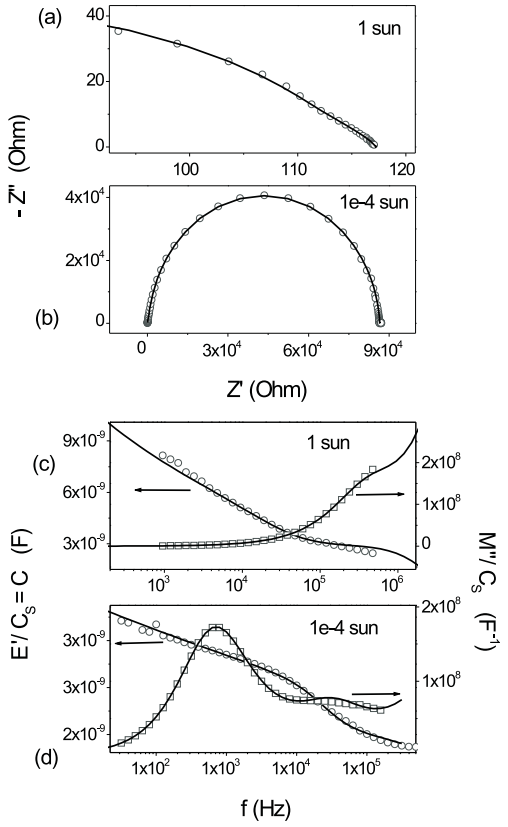

FIG. 6: (a-d) Examples of impedance spectra on a Z''-Z' plot for sample IV at 1 sun and 10^{-4} sun. (c-d) Real part of dielectric permittivity E' and imaginary part of electric modulus M'' versus frequency for the same data. Solid lines are fit to the model in Fig. 8(a).

Fig. 7

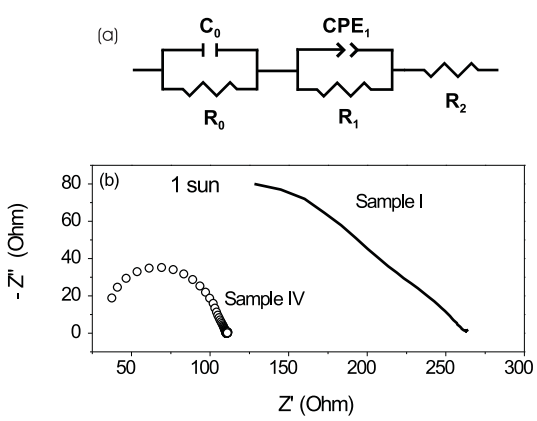

FIG. 7: (a) Simplified equivalent circuit for sample IV with improved back contact. (b) Comparison of impedance spectra on Z''-Z' plot for samples I and IV under 1 sun.

Fig. 8

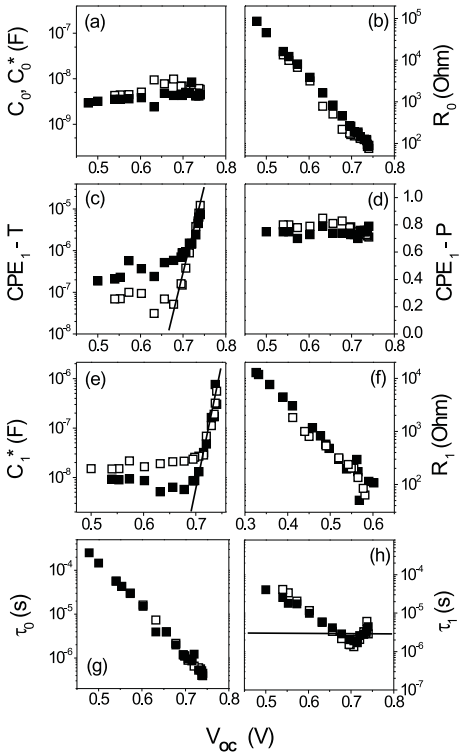

FIG. 8: (a-f) Equivalent circuit parameters against V_{oc} for sample IV, obtained from the fit of impedance data under varied illumination using the model in Fig. 8(a). Different symbols correspond to the two variations of the fitting procedures: ■ - with one CPE, □ - with two CPEs, see text. (g) Characteristic time of the first section $\tau_0(V_{oc})$. (h) $\tau_1^*(V_{oc}) = R_1 C_1^*$, corresponds to minority carrier lifetime at $V_{oc} > 0.65$ V. The straight solid lines are a guide for the eye.

Fig. 9

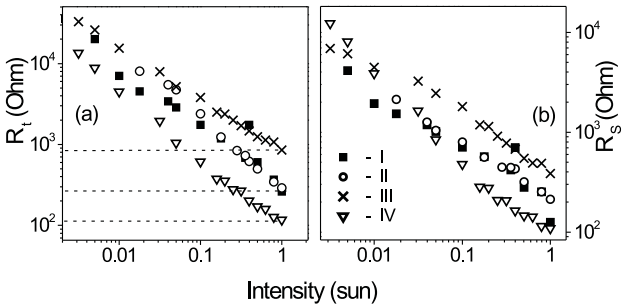

FIG. 9: Total (a) and series (b) resistance for samples I-IV versus light intensity. (■) - sample I, (○) - sample II, (×) - sample III, and (▽) - sample IV.

[1] Y. Y. Proskuryakov, K. Durose, B. M. Taele, S. Oelting, J. Appl. Phys. **102**, 024504 (2007).

[2] I. Mora-Seró, Y. Luo, G. Garcia-Belmonte, J. Bisquert, D. Muñoz, C. Voz, J. Puigdollers, R. Alcubilla, Solar En. Mat. and Solar Cells **92** 505 (2008).

[3] H. Bayhan, A. S. Kavasoğlu, Solar Energy **361**, 303 (2000); H. Bayhan, A. S. Kavasoğlu, Turk. J Phys. **27**, 529 (2003).

[4] I. Ferreira, L. Raniero, E.Fortunato, R. Martins, Thin Solid Films **511-512**, 390 (2006).

[5] L. Raniero, E. Fortunato, I. Ferreira, R. Martins, J. Non-Cryst. Solids **352**, 1880 (2006).

[6] G. Friesen, M. E. Özsan, E. D. Dunlop, Thin Solid Films **361**, 303 (2000).

[7] F. Fabregat-Sentiago, J. Bisquert, G. Garcia-Belmonte, G. Boschloo, A. Hagfeldt, Solar En. Mat. and Solar Cells **87**, 117 (2005).

[8] S. J. C. Irvine, V. Barrioz, D. Lamb, E. W. Jones and R. L Rowlands-Jones, J. Cryst. Growth **310**, 5198 (2008).

[9] Y. Y. Proskuryakov; K. Durose; J. D. Major; M. K. Al Turkestani; V. Barrioz; S. J. C. Irvine; E. W. Jones, Phys., submitted to Solar Eng. Mat. and Solar Cells.

[10] X. Wu, Solar Energy **77**, 803 (2004).

[11] V. Barrioz, S. J. C. Irvine, E. W. Jones, R. L. Rowlands, D. A. Lamb, Thin Solid Films **515**, 5808 (2007).

[12] Y. Y. Proskuryakov, J. D. Major, K. Durose, V. Barrioz, S. J. C. Irvine, E. W. Jones, D. Lamb, Appl. Phys. Lett. **91**, 153505 (2007).

[13] J. Ross MacDonald, "Impedance Spectroscopy, Emphasizing Solid Materials and Systems", John Wiley and Sons (1987).

[14] It should be mentioned that although parameter C_1 is known as a diffusion capacitance, it is also often referred to as a chemical capacitance. Strictly speaking, in case of a solar cell it describes a property of the system in equilibrium, and hence in general case it is not related to diffusion [J. Bisquert, Phys. Chem. Chem. Phys. **5**, 5360 (2003)].

[15] I. Mora-Seró *et al.*, Nano Lett. **6**, 640 (2006).

[16] L. A. Kosyachenko, E. V. Grushko, V. V. Motushchuk, Solar En. Mat. and Solar Cells **90**, 2201 (2006).

[17] Y. Y. Proskuryakov, K. Durose, B. M. Taele, S. Oelting, J. Appl. Phys. **101**, 014505 (2007).

[18] E. H. Rhoderick, "Metal Semiconductor Contacts", Oxford University Press (1978).

[19] I. Mora-Seró, G. Garcia-Belmonte, P. P. Boix, M. A. Vzquez and J. Bisquert, Energy Environ. Sci. (2008), in print.

[20] J. Bisquert, G. Garcia-Belmonte, A. Pitarch, Chem. Phys. Chem. **4**, 287 (2003).

[21] J. Bisquert, Phys. Rev. B **77**, 235203 (2008).